Civil Engineering Dimension
https://ced.petra.ac.id

A Study of the Partition of Unity-based T3-CNS and T3-DNS Finite Elements in Surface Fitting

Istiono, H.[1,2] and Wong, F.T.[1]*
[1] Department of Civil Engineering, Petra Christian University, Surabaya, INDONESIA
[2] Department of Civil Engineering, Adhi Tama Institute of Technology, Surabaya, INDONESIA

DOI: https://doi.org/10.9744/ced.28.1.11-22

Article Info:
Submitted: Mar 19, 2025
Reviewed: Apr 14, 2025
Accepted: July 01, 2025

Keywords:
partition of unity,
T3-CNS,
T3-DNS,
surface fitting.

Corresponding Author:
Wong, F.T.
Department of Civil Engineering,
Petra Christian University, Surabaya,
INDONESIA
Email: wftjong@petra.ac.id

Abstract

Various alternative, enhanced finite element methods (FEMs) have been proposed to improve the accuracy and convergence of traditional FEM. One promising approach is the hybrid FEM-meshfree method using the partition of unity concept. This study examines the performance of two variants of the hybrid-meshfree method: the three-node triangular element with continuous nodal stress (T3-CNS) and the three-node triangular element with discontinuous nodal stress (T3-DNS). These methods are evaluated in the context of surface fitting through numerical tests. Their accuracy and convergence are compared with the standard triangular element and Kriging-based FEM. The results show that both T3-CNS and T3-DNS methods maintain consistency and yield accurate surface approximations with good convergence. However, their performance declines in problems involving gradient singularities. This study enhances the understanding of T3-CNS and T3-DNS interpolations, providing insights into their application in a Galerkin method for solving engineering model problems.

INTRODUCTION

The finite element method (FEM) is a widely used numerical method for solving mathematical model problems in the field of engineering. In its application, FEM users often prefer to use low-order elements, such as four-node quadrilateral elements and three-node triangular elements. However, the accuracy of these low-order elements in predicting stress (or generally the gradient of primary variables) is relatively low, due to the discontinuity of resulting stresses along the element boundaries. Furthermore, the accuracy of these elements is also quite sensitive to the distortion of element shapes [1].

To address the weaknesses of the FEM, alternative methods known as mesh-free methods have been developed since the early 1990s. These include the element-free Galerkin method [2], the reproducing kernel particle method [3], and the meshfree local Petrov-Galerkin method [4] (see [5] for the details of various meshfree methods). Compared to traditional FEM, mesh-free methods generally produce smoother and more accurate stress distributions. However, they also have some drawbacks. Some mesh-free methods have difficulty in imposing the essential boundary conditions because their approximation functions do not possess the Kronecker delta property. In addition, the computational cost associated with mesh-free methods is significantly higher than that of the standard FEM.

Over the past two decades, researchers have developed a class of methods that combine the advantages of FEM and mesh-free methods using the partition of unity method [6]. In these approaches, the approximation function is constructed by combining a set of weight functions with local approximation functions used in various mesh-free

Note : Discussion is expected before July, 1st 2026, and will be published in the "Civil Engineering Dimension", volume 28, number 2, September 2026.
ISSN : 1410-9530 print / 1979-570X online
Published by : **Petra Christian University**

methods. These weight functions sum to one within the problem domain and are referred to as the partition of unity (PU). Some of the earliest PU-based methods that combine FEM and mesh-free methods include quadrilateral element 'FE-Meshfree' [7], hexahedral element based on the PU [8], quadrilateral element with continuous nodal stress [9], triangular element 'FE-Meshfree' [10], and triangular element with continuous nodal stress (T3-CNS) [11].

Among the various PU-based 'FE-meshfree' methods, we are particularly interested in the T3-DNS and T3-CNS elements [11]. The approximate functions for the T3-DNS elements are constructed by combining linear triangular element shape functions with constrained and orthonormalized least squares (CO-LS) approximations. On the other hand, approximate functions for the T3-CNS elements are created by combining continuous nodal gradient weight functions as the PU and CO-LS approximations. The CO-LS approximation is a least-squares approximation with an orthonormalized polynomial basis to avoid inverting the least-squares moment matrix. Furthermore, this approximation function is constrained to satisfy the Kronecker delta property at the element nodes [9,11].

The T3-DNS and T3-CNS elements offer several advantages: first, they inherit the high convergence rate and accuracy properties of mesh-free methods. Second, they are less sensitive to element shape distortion compared to standard triangular finite elements [11,12]. Furthermore, the use of triangular elements for a geometrically complex problem domain is easier for automatic mesh generation and adaptivity compared to the use of quadrilateral elements. The T3-CNS element, which maintains gradient continuity at the element nodal points, can produce a smoother global gradient field than the T3-DNS.

The T3-CNS and T3-DNS elements have been applied to the static and free vibration of plane elasticity model problems [12], crack analysis [13], and geometric nonlinear solid mechanics problems [14]. However, the performance of the T3-CNS and T3-DNS interpolations, specifically their consistency, accuracy, and convergence in approximating mathematically defined surfaces, have not been examined in previous works. Therefore, this paper aims to present a numerical study on the performance of the T3-CNS and T3-DNS interpolations and their derivatives in surface fitting. This study closely follows the approach of Wong *et al.* [15,16]. It aims to provide valuable insights into the interpolation characteristics of the T3-CNS and T3-DNS elements.

T3-CNS AND T3-DNS INTERPOLATIONS

We analyzed a two-dimensional problem domain, denoted as Ω. To construct either the T3-CNS or T3-DNS interpolation, as is typically done in usual FEM, the domain Ω is partitioned into a mesh of three-node triangular elements, referred to as Ω^h. The approximation of a surface function z (or other field variables) over a typical triangular element $\overline{\Omega}^e \subset \Omega^h$ is expressed as

$$z \approx z^h = \sum_{i=1}^{3} w_i(L_1, L_2, L_3) z_i(x, y) \tag{1}$$

In this equation, $w_i(L_1, L_2, L_3)$ represents the weight function associated with node i, which is expressed in terms of triangular area coordinates L_1, L_2, and L_3. The function $z_i(x, y)$ is the local approximation centered at node i. It is worth noting that if z_i is taken as a nodal value at node i, the approximation z^h reduces to the standard finite element approximation.

Weight Functions

The weight functions for the T3-CNS element are given as [11]:

$$w_1 = L_1 + L_1^2 L_2 + L_1^2 L_3 - L_1 L_2^2 - L_1 L_3^2 \tag{2a}$$

$$w_2 = L_2 + L_2^2 L_3 + L_2^2 L_1 - L_2 L_3^2 - L_2 L_1^2 \tag{2b}$$

$$w_3 = L_3 + L_3^2 L_1 + L_3^2 L_2 - L_3 L_1^2 - L_3 L_2^2 \tag{2c}$$

Conversely, the weight functions for the T3-DNS element are identical to the linear shape functions of three-node triangular elements, that is,

$$w_1 = L_1; w_2 = L_2; w_3 = L_3 \tag{3}$$

The T3-CNS and T3-DNS weight functions exhibit several similarities. Firstly, they both satisfy the partition of unity property, that is, $\sum_i w_i = 1$. Secondly, their values within the support domain range between 0 and 1, i.e., $0 \le w_i \le 1$.

Thirdly, both sets of weight functions possess the Kronecker delta property. A key difference between them lies in their continuity. The T3-CNS weight functions are C^0 continuous along the element boundaries and C^1 continuous at the element nodal points. In contrast, the T3-DNS weight functions are C^0 continuous at every point along the element boundaries, including the nodal points. In other words, the gradients of the T3-CNS weight functions are continuous at the nodal points while those of the T3-DNS weight functions are discontinuous at these points.

Nodal Approximations

The nodal approximation $z_i(x, y)$ is established using a constrained and orthonormalized least-squares (CO-LS) approximation method [9,11,17]. To construct a CO-LS nodal approximation at a node i, we need to define the support of node i (denoted as $\overline{\Omega}_i$). For a CO-LS with a quadratic basis function, $\overline{\Omega}_i$ It is defined as the region surrounding node i that encompasses all the elements sharing this node. Node i is referred to as the central node, while the other connected nodes are referred to as satellite nodes. For example, Figure 1(a) shows the support of node 1 of element number e encompassing six triangular elements that share node 1 (the central node), covering the six satellite nodes 2, 3, 4, 5, 6, and 7.

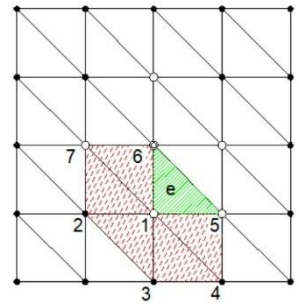

(a) Nodal Support of Node 1

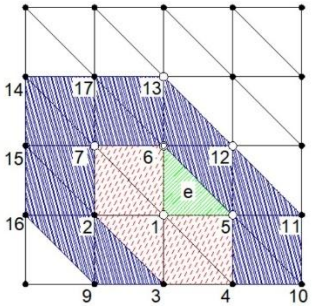

(b) Two-layer Nodal Support of Node 1

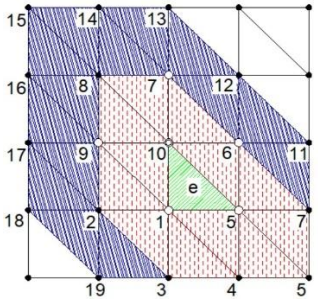

(c) Enlarged Two-layer Nodal Support of Node 1 and Element Support of Element Number e

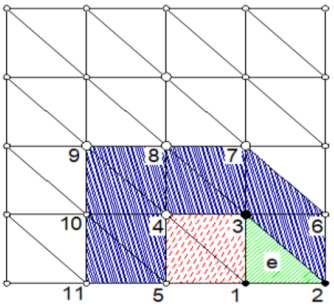

(d) Nodal Support of Node 1 If a Central Node is Located at the Boundary

Figure 1. (a) Support of node 1 of element number e, covering the green and red shaded elements around node 1; (b) Two-layer support of node 1 of element number e, covering the green, red, and blue shaded elements around node 1; (c) Enlarged two-layer support of node 1, and also element support of element number e, covering two layers of elements surrounding element number e; (d) Two-layer support of boundary node 1 of element number e at the corner, covering the green, red, and blue shaded elements around node 1.

Consider a nodal support $\overline{\Omega}_i$ with n supporting nodes. Let the numbering labels for the nodes in the support be j, j = 1, …, n. The CO-LS approximation around node i can be written as

$$z_i(x,y) = \mathbf{\Phi}_i(x,y)\mathbf{z}_i = \sum_{j=1}^{n} \phi_j^{[i]}(x,y) z_j \tag{4}$$

$$\mathbf{\Phi}_i(x,y) = \left[\phi_1^{[i]}(x,y) \quad \phi_2^{[i]}(x,y) \quad \cdots \quad \phi_n^{[i]}(x,y)\right] = \mathbf{r}^{\mathrm{T}}(x,y)\mathbf{B}^{[i]} \tag{5}$$

In these equations, $\varphi_j^{[i]}$ is the CO-LS shape function for the local approximation centered at node i, associated with node j, and the vector

$$\mathbf{z}_i = \{z_1 \quad z_2 \quad \cdots \quad z_n\}^T \tag{6}$$

is the n×1 vector of nodal values z_j at the supporting nodes. The vector $\mathbf{r}(x, y)$ represents the orthonormalized polynomial basis vector. This vector is obtained by orthonormalizing a polynomial basis vector $\mathbf{p}(x, y)$ using the Gram-Schmidt algorithm [9,11,17]. In this study, the basis function used is either a quadratic polynomial basis, viz.

$$\mathbf{p}(x,y) = [1 \quad x \quad y \quad x^2 \quad xy \quad y^2]^{\mathrm{T}} \tag{7a}$$

or a cubic polynomial basis, viz.

$$\mathbf{p}(x,y) = [1 \quad x \quad y \quad x^2 \quad xy \quad y^2 \quad x^3 \quad x^2y \quad xy^2 \quad x^3]^{\mathrm{T}} \tag{7b}$$

The matrix $\mathbf{B}^{[i]}$ is defined as follows:

$$\mathbf{B}^{[i]} = \left[\mathbf{B}_1^{[i]} \quad \mathbf{B}_2^{[i]} \quad \cdots \quad \mathbf{B}_n^{[i]}\right] \tag{8a}$$

$$\mathbf{B}_j^{[i]} = \mathbf{r}(x_j, y_j) - f_j^{[i]}\mathbf{r}(x_i, y_i) \tag{8b}$$

$$f_j^{[i]} = \begin{cases} \dfrac{\mathbf{r}^{\mathrm{T}}(x_i,y_i)\mathbf{r}(x_j,y_j)}{\mathbf{r}^{\mathrm{T}}(x_i,y_i)\mathbf{r}(x_i,y_i)} & \text{if } j \neq i \\ \dfrac{\mathbf{r}^{\mathrm{T}}(x_i,y_i)\mathbf{r}(x_j,y_j)-1}{\mathbf{r}^{T}(x_i,y_i)\mathbf{r}(x_i,y_i)} & \text{if } j = i \end{cases} \tag{8c}$$

A detailed derivation of the CO-LS approximation within the framework of a more general moving least-squares approximation is presented in Ref. [17]. It is worth noting that the number of nodes in the nodal support, n, may vary for each central node i = 1, 2, 3.

To construct a proper CO-LS approximation, the number of supporting nodes, n, must be at least equal to the number of polynomial basis terms, m. This means $n \geq 6$ for a quadratic basis CO-LS approximation and $n \geq 10$ for a cubic basis. Consequently, when employing a cubic basis, the nodal support of node 1 shown in Figure 1(a) must be extended to include a second layer of surrounding nodes, as depicted in Figure 1(b). This creates a two-layer nodal support comprising 16 nodes. However, numerical tests revealed that even with this extended nodal support, the CO-LS approximation with a cubic basis could not be properly constructed. This issue is resolved by merging the two-layer nodal supports of all central nodes of element e, as depicted in Figure 1(c), thereby expanding the nodal support to encompass two layers of surrounding elements of element e.

If an element e is positioned at a corner, one or more nodal support domains may contain fewer than 6 nodes when using a quadratic polynomial basis to construct the CO-LS shape functions. To solve this problem, a two-layer nodal support will be employed for a corner element, as illustrated in Figure 1(d).

T3-CNS AND T3-DNS SHAPE FUNCTIONS

In order to combine the weight functions $w_i(L_1, L_2, L_3)$, i = 1, 2, 3, and the CO-LS shape functions $\phi_j^{[i]}$, j = 1, 2, ..., n, the support of element e, $\widehat{\Omega}^e$, is defined as the union of the three nodal supports, i.e. $\widehat{\Omega}^e = \overline{\Omega}_1 \cup \overline{\Omega}_2 \cup \overline{\Omega}_3$. Let the nodal numbering in $\widehat{\Omega}^e$ be I = 1, 2, ..., N, where N is the total number of nodes in the element support. For example, Figure 2(a) shows the support of element e, which covers 12 nodes (N = 12). Referring to this element numbering system and substituting Equation (4) into Equation (1), the approximate surface function can be expressed as

$$z^h = \sum_{I=1}^{N} \psi_I(x,y) z_I \tag{9a}$$

$$\psi_I(x,y) = \sum_{i=1}^{3} w_i(L_1, L_2, L_3)\, \phi_I^{[i]}(x,y) \tag{9b}$$

where $\psi_I(x, y)$ is the T3-CNS or T3-DNS shape function associated with node I. In Equation (9b), if node I is not in the nodal support of node i, then $\varphi_I^{[i]}$ is defined as zero. It is obvious that the T3-CNS or T3-DNS shape function is a linear combination of the weight functions and the CO-LS shape functions.

For T3-CNS or T3-DNS shape functions of an element number e with cubic-based CO-LS nodal approximations, the support of element e coincides with its enlarged nodal supports, as illustrated in Figure 1(c). The element support for a corner element, formed by the union of two-layer supports of central nodes i = 1, 2, 3, is shown in Figure 2(b).

The T3-CNS and T3-DNS shape functions and their corresponding approximation functions possess desirable properties that make them suitable to be employed as trial and test functions in the Galerkin FEM. Firstly, they have a consistency (or reproducibility) property, that is, the T3-CNS and T3-DNS approximation functions can exactly reproduce polynomial functions up to the same degree as their basis functions. This property will be verified numerically in the following section. Secondly, the T3-CNS and T3-DNS approximation functions inherit the

conformity (inter-element continuity) property from their weight functions. Thus, both are C^0-continuous along inter-element boundaries. Moreover, the T3-CNS function is C^1-continuous at nodal points.

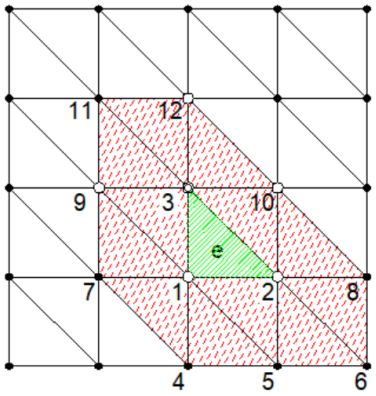

(a) One-layer Element Support

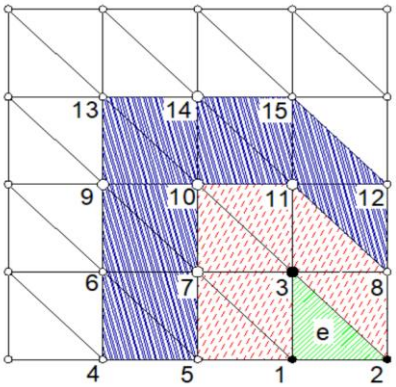

(b) Two-layer Element Support for a Corner Element

Figure 2. Support of Element *e*, Encompassing the Shaded Area Around Element *e* and Element *e* Itself

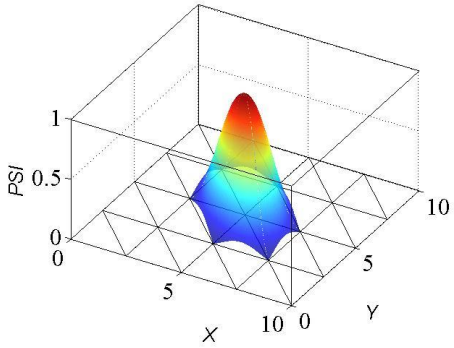

Figure 3. T3-CNS Shape Function Associated with Node Number 13

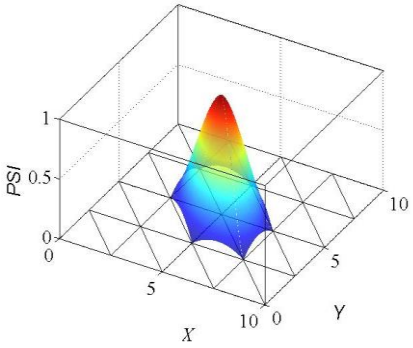

Figure 4. T3-DNS Shape Functions Associated with Node Number 13

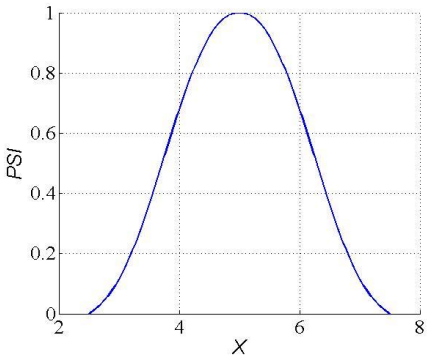

Figure 5. T3-CNS Shape Functions along Line $Y = 5$ (see Figure 3)

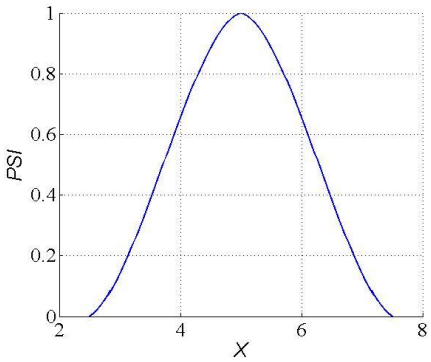

Figure 6. T3-DNS Shape Functions along Line $Y = 5$ (see Figure 4)

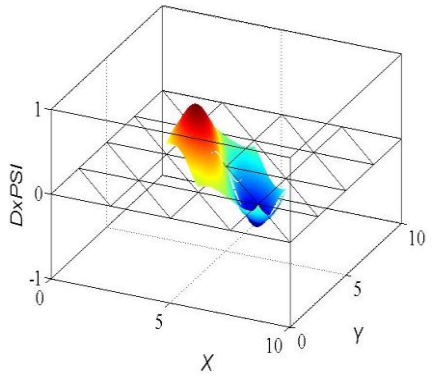

Figure 7. Partial Derivative with respect to *X* of the T3-CNS Shape Function associated with Node Number 13

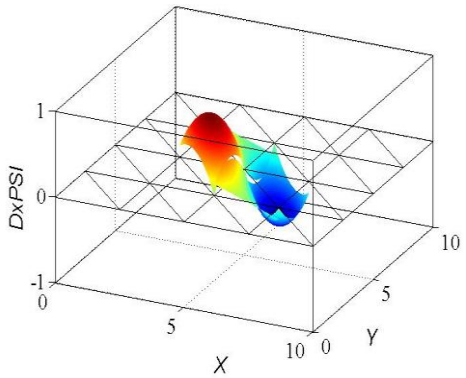

Figure 8. Partial Derivative with respect to *X* of the T3-DNS Shape Functions associated with Node Number 13

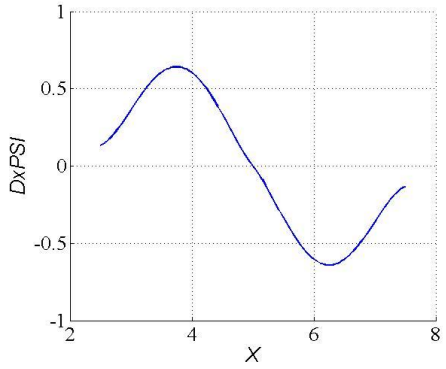

Figure 9. Partial Derivative with respect to X of the T3-CNS Shape Function along Line $Y = 5$ (see Figure 7)

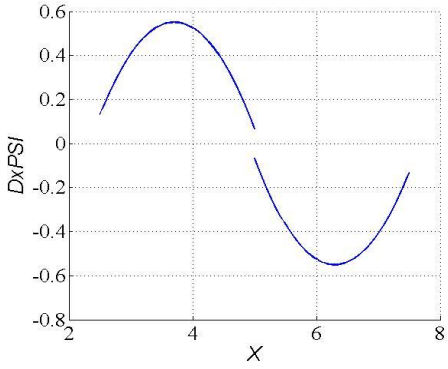

Figure 10. Partial Derivative with respect to X of the T3-DNS Shape Function along Line $Y = 5$ (see Figure 8)

Figures 3 and 4 show graphs of the T3-CNS and T3-DNS shape functions, respectively, associated with the square central node. Figures 5 and 6 depict section plots along line $Y = 5$. The partial derivatives of the shape functions with respect to X and their sections along line $Y = 5$ are displayed in Figures 7 to 10. It is evident that the derivative of the T3-DNS shape function exhibits a discontinuity at the nodal point, while the derivative of the T3-CNS is continuous at the nodal point.

Note: In Figures 3 to 10, *PSI* is a T3-CNS or T3-DNS shape function as given in Equation (9b). *DxPSI* represents the partial derivative of *PSI* with respect to X. Due to the limitation of symbols in the MATLAB environment, 'ψ' and '$\psi_{,x}$' were written as '*PSI*' and '*DxPSI*', respectively.

NUMERICAL TESTS

A series of numerical tests is conducted to evaluate the consistency property, accuracy, and convergence of the T3-CNS and T3-DNS interpolations and their derivatives on surface fitting of $z = f(x, y)$. The approximation error is measured using the relative L_2 *n*orm of error, that is,

$$r_z = \sqrt{\frac{\int_{\Omega^h}(z^h - z)^2 dA}{\int_{\Omega^h} z^2 dA}} \tag{10}$$

where z^h is the surface function approximation (the fitted surface). This error norm is also used to measure the relative error of the partial derivatives of the function (by replacing z and z^h with their derivatives). The integral in Equation (10) is evaluated numerically using the Gaussian quadrature rule for triangular elements with the six-point quadrature rule. The results are then compared to those obtained using the standard triangular element interpolation (T3) and the Kriging-based triangular element interpolation with a quadratic basis or a cubic basis and the quartic spline correlation function (K-FEM) [18].

It is worth mentioning that Kriging-based FEM is an enhancement of classical FEM by utilizing Kriging interpolation as the trial and test functions, in place of polynomial interpolation. The Kriging interpolation is constructed by employing a set of nodes within a specified domain of influencing nodes (DOI), which includes the element itself and several layers of neighboring elements [16,18]. Both the T3-CNS and T3- DNS methods share a similarity with the K-FEM in that they employ a DOI for constructing their interpolation. The DOI is identical to the element support in the T3-CNS and T3-DNS methods. Therefore, it is worthwhile to compare the performance of these two interpolation schemes with the K-FEM interpolation.

Consistency Property

An interpolation scheme that can exactly represent all polynomial terms of degree m is referred to as m-consistent. As a quadratic or a cubic polynomial basis is used in this study to construct the T3-CNS and T3-DNS interpolations, they are expected to be able to reproduce a quadratic function or a cubic function, respectively. To examine this consistency property, we utilize a unit square domain that has been partitioned using both a regular mesh and an irregular mesh of triangular elements, as shown in Figures 11(a) and (b), respectively. The functions considered are the bases of a cubic polynomial: $z = 1$, $z = x$, $z = y$, $z = x^2$, $z = xy$, $z = y^2$, $z = x^3$, $z = xy^2$, $z = x^2y$, and $z = y^3$.

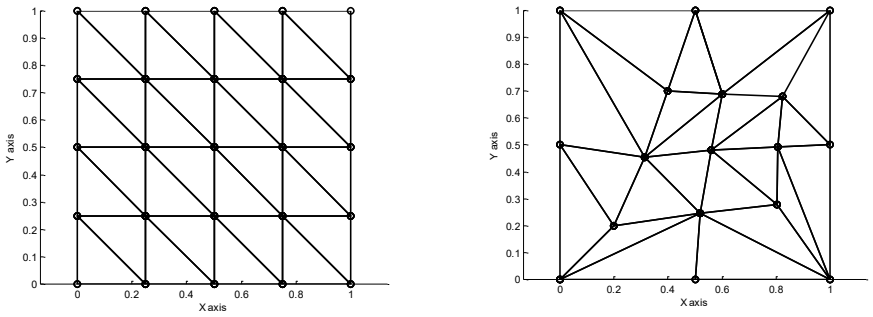

(a) Regular mesh (b) Irregular mesh

Figure 11. Square Function Domain with (a) A Regular Mesh of Triangular Elements and (b) An Irregular Mesh of Triangular Elements

Table 1 presents the relative errors of the T3-CNS and T3-DNS interpolations using a quadratic basis, applied to the irregular mesh shown in Figure 11(b). For brevity, similar results regarding the interpolations using the regular mesh shown in Figure 11(a), as well as the results for the T3-CNS and T3-DNS interpolations using a cubic basis, are not included here.

Table 1. Relative Errors of Various Approximation Functions with a Quadratic Basis on the Irregular Mesh Shown in Figure 11(b)

Function	T3-CNS	T3-DNS	K-FEM	T3
1	1,110E-15	1,096E-15	1,786E-16	5,604E-16
x	1,354E-15	1,377E-15	1,859E-16	6,545E-16
y	1,572E-15	1,578E-15	1,622E-16	5,439E-16
xy	1,008E-15	1,004E-15	2,413E-16	4,680E-02
x^2	9,570E-16	9,310E-16	1,483E-16	4,097E-01
y^2	1,476E-15	1,431E-15	1,821E-16	6,830E-02
x^3	3,790E-02	3,780E-02	2,434E-02	9,838E-02
y^3	4,568E-02	4,533E-02	2,530E-02	1,527E-01
xy^2	2,486E-02	2,452E-02	1,720E-02	1,023E-01
x^2y	1,871E-02	1,844E-02	1,471E-02	7,228E-02

The results show that the relative errors of the T3-CNS and T3-DNS interpolations with a quadratic basis, along with their partial derivatives, are of the order of −16 to −14 when approximating polynomial basis functions and their partial derivatives up to quadratic bases. Furthermore, we found that the relative errors of the T3-CNS and T3-DNS interpolations with a cubic basis, along with their partial derivatives, are also of the orders −16 to −14. These errors are due to the CO-LS computation and numerical round-off errors, not interpolation errors. Thus, it is evident that the T3-CNS and T3-DNS interpolations with a quadratic basis are quadratically consistent, while those with a cubic basis are cubically consistent.

For comparison, the K-FEM interpolation has also been shown to be consistent. As expected, the T3 interpolation can reproduce exact solutions only up to linear basis functions. Of course, none of these interpolations can exactly reproduce polynomials of a higher degree than their respective polynomial bases.

Accuracy and Convergence

To examine the accuracy and convergence of the T3-CNS and T3-DNS interpolations in surface fitting, we employ a quadratic function [16] , a bi-cosine function [15], and a spherical function, which are respectively defined as follows:

$$z = 1 - x^2 - y^2 \tag{11}$$

$$z = \cos\left(\frac{\pi}{2}x\right)\cos\left(\frac{\pi}{2}y\right) \tag{12}$$

$$z = \sqrt{1 - x^2 - y^2} \tag{13}$$

The quadratic function (Equation (11)) and bi-cosine function (Equation (12)) are defined over two different domains, namely,

$$\widehat{\Omega}_S = \{(x, y) | 0 \le x \le 1, 0 \le y \le 1\} \tag{14}$$

$$\widehat{\Omega}_C = \{(x,y)|x^2 + y^2 \leq 1, x \geq 0, y \geq 0\} \quad (15)$$

The domain of the spherical function (Equation (13)) is naturally defined by Equation (15). It is important to note that the spherical function has a singularity in its radial gradient along the circular boundary.

Equation (14) represents a unit square, while Equation (15) represents a quarter of a unit circle. The unit square is partitioned using regular triangular meshes of 4×4 (as shown in Fig. 11(a)), 8×8, 16×16, and 32×32. On the other hand, the quarter circle is partitioned using triangular meshes of 3×1×1, 3×2×2, 3×4×4, and 3×8×8, as shown in Figure 12.

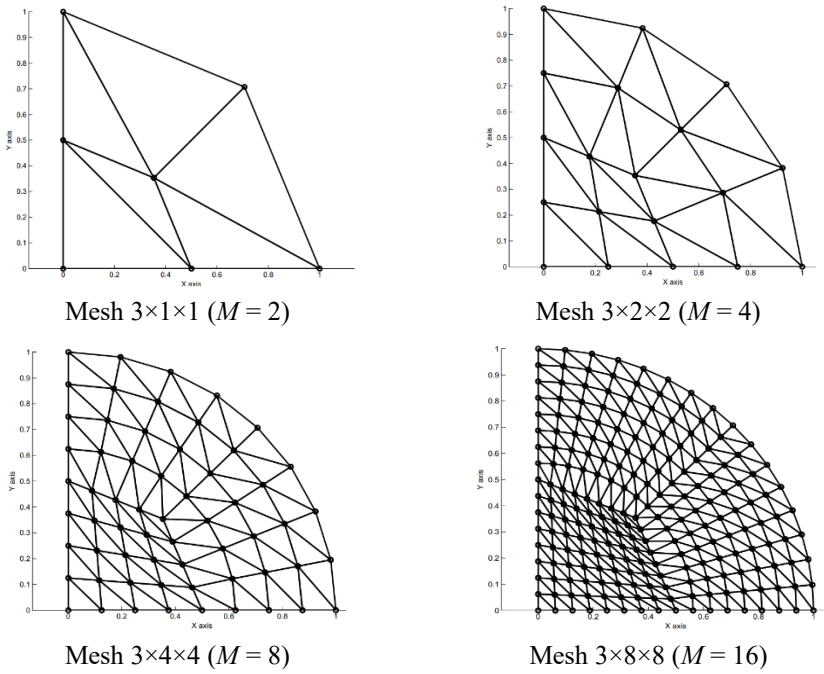

Mesh 3×1×1 (M = 2) Mesh 3×2×2 (M = 4)

Mesh 3×4×4 (M = 8) Mesh 3×8×8 (M = 16)

Figure 12. A Quarter-circular Domain Divided into Triangular Elements (M: Number of Elements on Each Side)

Quadratic Surface Fitting

Relative errors in fitting the quadratic function (Equation 11) and its partial derivatives over the quarter circular domain, for the T3-CNS and T3-DNS interpolations using a quadratic basis, are presented in Tables 2 and 3. Similar results are observed for the quadratic surface fitting over the square domain, as well as for the surface fitting using the cubic-based T3CNS and T3-DNS interpolations over the square and circular domains (for brevity, the results are not included here).

Table 2. Relative Errors of Quadratic Function Approximation (r_z) over the Quarter Circular Domain using Quadratic Basis Interpolations (except T3)

Mesh (M)	r_z			
	T3-CNS	**T3-DNS**	**K-FEM**	**T3**
2	4,23E-16	3,90E-16	1,53E-16	1,70E-01
4	7,32E-16	3,77E-15	1,95E-16	4,60E-02
8	5,15E-15	5,08E-15	2,44E-16	1,18E-02
16	1,90E-14	1,89E-14	4,08E-16	2,99E-03

M: number of elements on each domain side

Table 3. Relative Errors for Approximation of the Partial Derivatives with respect to x ($r_{z,x}$) and y ($r_{z,y}$) of the Quadratic Function over the Quarter Circular Domain using Quadratic Basis Interpolations (except T3)

Mesh	*rz,x*				*rz,y*			
(M)	**T3-CNS**	**T3-DNS**	**K-FEM**	**T3**	**T3-CNS**	**T3-DNS**	**K-FEM**	**T3**
2	2,09E-15	1,87E-15	3,30E-16	3,74E-01	1,05E-15	1,03E-15	2,15E-16	3,74E-01
4	3,95E-15	3,77E-15	5,91E-16	1,75E-01	3,64E-15	3,50E-15	6,40E-16	1,75E-01
8	6,60E-14	6,81E-14	1,76E-15	8,63E-02	7,49E-14	7,63E-14	1,59E-15	8,63E-02
16	5,17E-13	5,49E-13	8,70E-15	4,30E-02	5,56E-13	5,91E-13	7,31E-15	4,30E-02

The results demonstrate that, as expected, the T3-CNS, T3-DNS, and K-FEM interpolations with both quadratic and cubic bases can effectively reproduce the given quadratic function. The findings again confirm the consistency (reproducibility) property of the T3-CNS, T3-DNS, and Kriging interpolations. In contrast, the T3 interpolation cannot reproduce the quadratic function. This also applies to partial derivative functions with respect to x and y in Table 3. Nevertheless, the results from T3 interpolation converge monotonically to the quadratic surface as the mesh is refined. The order of convergence for the T3 interpolation over the square and circular domains and its partial derivatives are close to 2 and 1, which are the theoretical order of convergence for a piecewise linear interpolation [19,10].

Bi-cosine Surface Fitting

Figure 13 depicts log-log scaled graphs of the relative errors of the T3-CNS and T3-DNS interpolations and their partial derivatives using a cubic basis to fit the bi-cosine function over a quarter of the unit circular domain (to save space similar graphs for the square domain are not shown here). The horizontal axis represents the mesh fineness levels, characterized by the number of elements along each edge of the domain, denoted as M.

The results indicate that both the T3-CNS and T3-DNS interpolations exhibit good accuracy and convergence. The accuracy and order of convergence of the T3-CNS and T3-DNS interpolations are virtually identical, achieving approximately one order of magnitude more accurate than the linear T3 interpolation. Furthermore, the partial derivative interpolations are about two orders of magnitude more accurate than the T3 interpolation derivatives. The T3-CNS and T3-DNS interpolations are, however, less accurate and exhibit a slower convergence rate when compared to the K-FEM interpolation.

Spherical Surface Fitting

Relative errors of cubic-based T3-CNS and T3-DNS interpolations in approximating the spherical function (as expressed in Equation (13)) and its partial derivatives are presented in Figure 14. The results show that their accuracy and convergence rate are not as good as when they were applied to the bi-cosine function. Increasing the basis degree from quadratic to cubic does not lead to a significant improvement in either accuracy or convergence (relative errors of quadratic-based not present here to save space).

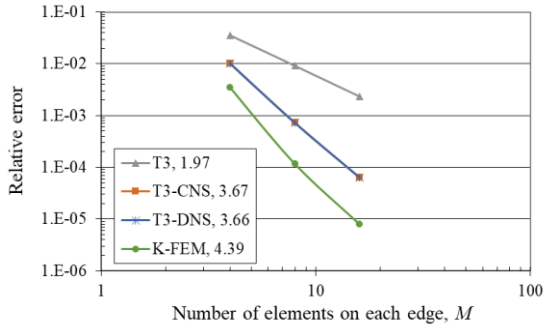

(a) Relative Errors of Fitting the Bi-Cosine Function over a Quarter of the Circular Domain

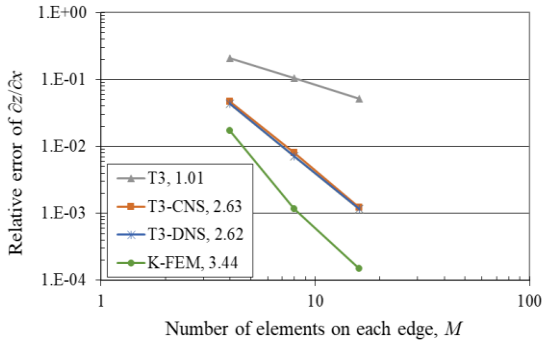

(b) Relative Errors of Fitting the Bi-Cosine Function Partial Derivative with respect to X over a Quarter of the Circular Domain

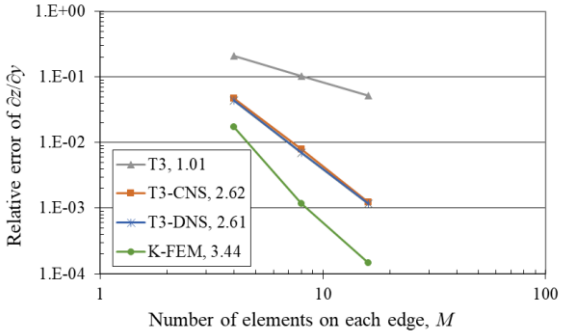

(c) Relative Errors of Fitting the Bi-Cosine Function Partial Derivative with respect to Y over a Quarter of the Circular Domain

Figure 13. Log-log scaled graphs of the relative errors of bi-cosine surface fitting and their partial derivatives over a quarter of the circular domain using different cubic-based interpolation schemes (except the T3). The numbers in the legend indicate the average order of convergence

In contrast to the previous findings, the orders of convergence of the T3-CNS, T3-DNS, and K-FEM interpolations, along with their partial derivatives, are lower than those of the T3 interpolation. Moreover, the partial derivatives produced by the T3-CNS and T3-DNS interpolations are less accurate than those of the T3 interpolation, with the exception of the mesh of $M = 2$ with quadratic-based interpolations.

The reason for the poor performance of the T3-CNS and T3-DNS interpolations is the presence of a radial gradient singularity along the circular boundary of the problem domain. This phenomenon has been documented for the K-FEM interpolation in previous work by Wong and Kanok-Nukulchai [16]. Therefore, the T3-CNS and T3-DNS element interpolations are not well-suited for approximating problems that involve a gradient singularity.

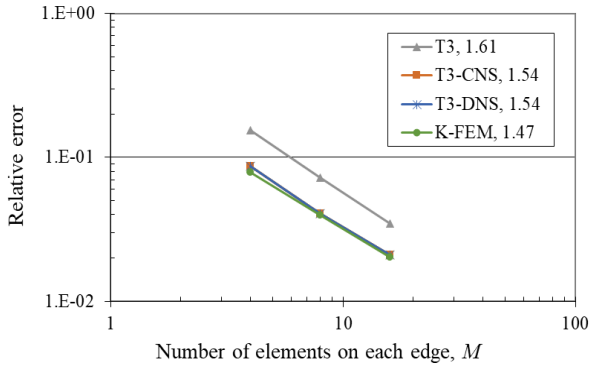

(a) Relative Errors of Fitting the Spherical Function over a Quarter of the Circular Domain

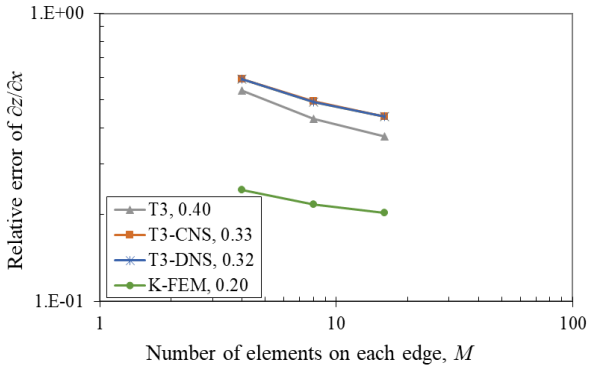

(b) Relative Errors of Fitting the Spherical Function Partial Derivative with respect to X over a Quarter of the Circular Domain

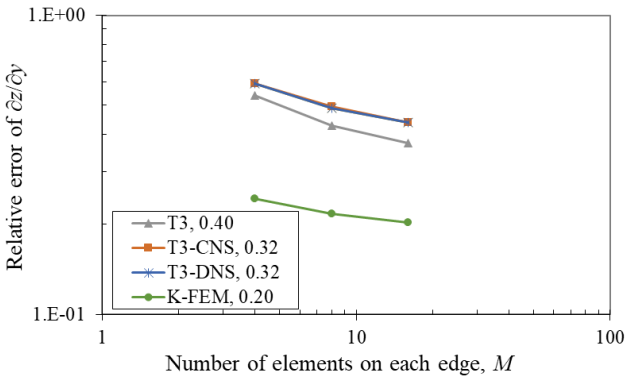

(c) Relative Errors of Fitting the Spherical Function Partial Derivative with respect to Y over a Quarter of the Circular Domain

Figure 14. Log-log scaled graphs of the relative errors of spherical surface fitting and their partial derivatives over a quarter of the circular domain using different cubic-based interpolation schemes (except the T3). The numbers in the legend indicate the average order of convergence

Remarks on K-FEM Interpolation

The numerical tests indicated that the K-FEM interpolation is superior in surface fitting compared to the T3-CNS and T3-DNS interpolations. This suggests that the K-FEM interpolation is better suited to serve as the trial function in a Galerkin FEM. However, it is important to note that the K-FEM interpolation is discontinuous along the element boundaries (non-conforming). While this nonconformity does not affect surface fitting, it could adversely affect the convergence rate in the Galerkin FEM [18].

CONCLUSIONS

A series of numerical tests have been conducted to evaluate the consistency, accuracy, and convergence properties of T3-CNS and T3-DNS finite element interpolations. The results show that these interpolations are consistent for both irregular and regular meshes, which is also true for K-FEM interpolation. The T3-CNS and T3-DNS interpolations with quadratic and cubic bases demonstrated high accuracy and good convergence in fitting quadratic and bi-cosine surfaces. The accuracy of T3-CNS and T3-DNS interpolations is significantly better than that of standard triangular element interpolation. However, their accuracy and convergence rates are lower compared to

those of K-FEM interpolation. Additionally, when applied to spherical surface fitting, their performance was less satisfactory due to the presence of a radial gradient singularity. Since T3-CNS and T3-DNS interpolations possess consistency properties and exhibit good accuracy and convergence for smooth gradient functions, they are viable alternatives for use as trial solutions in Rayleigh-Ritz or Galerkin finite element methods.

Overall, this study enhances the understanding of the interpolation characteristics of T3-CNS and T3-DNS elements, providing valuable insights for their application in engineering analysis. Future research could explore the potential applications of T3-CNS and T3-DNS finite elements in various engineering problems.

REFERENCES

1. Lee, N.S. and Bathe, K.J., Effects of Element Distortions on the Performance of Isoparametric Elements, *International Journal for Numerical Methods in Engineering,* 36, 1993, pp. 3553-3576. doi: 10.1002/nme.1620362009.
2. Belytschko, T., Lu, Y.Y., and Gu, L., Element-free Galerkin, *International Journal for Numerical Methods in Engineering*, 37(02), 1994, pp. 229–256. doi: 10.1002/nme.1620370205.
3. Liu, W., Jun, S., and Zhang, Y., Reproducing Kernel Particle Methods, *International Journal for Numerical Methods in Engineering,* 20(8-9), 1995, pp. 1081–106. doi: 10.1002/fld.1650200824.
4. Atluri, S. and Zhu, T., New Meshless Local Petrov–Galerkin (MLPG) Approach in Computational Mechanics, *Computational Mechanics,* 22(2), 1998, pp. 17–27. doi: 10.1007/s004660050346.
5. Liu, G.R., *Meshfree Methods: Moving Beyond the Finite Element Method*, Second Edition, Boca Raton: Taylor and Francis Group, 2009.
6. Babuška, I. and Melenk, J.M., The Partition of Unity Method, *International Journal for Numerical Methods in Engineering,* 40(4), 1997, pp. 727-758. doi: 10.1002/(sici)1097-0207(19970228)40:4<727::aid-nme86>3.0.co;2-n.
7. Rajendran, S. and Zhang, B.R., A ‘‘FE-meshfree’’ QUAD4 Element Based on Partition of Unity, *Computer Methods in Applied Mechanics and Engineering,* 197(1-4), 2007, pp. 128–147. doi: 10.1016/j.cma.2007.07.010.
8. Ooi, E., Rajendran, S., Yeo, J., and Zhang, B., A Mesh Distortion Tolerant 8-Node Solid Element Based on the Partition of Unity Method with Inter-element Compatibility and Completeness Properties, *Finite Elements in Analysis and Design,* 43(10), 2007, pp. 771–787. doi: 10.1016/j.finel.2007.05.008.
9. Tang, X.H., Zheng, C., Wu, S.C., and Zhang, J.H., A Novel Four-node Quadrilateral Element with Continuous Nodal Stress, *Applied Mathematics and Mechanics,* 30(12), 2009, pp. 1519–1532. doi: 10.1007/s10483-009-1204-1.
10. Xu, J.P. and Rajendran, S., A ‘FE-Meshfree’ TRIA3 Element Based on Partition of Unity for Linear and Geometry Nonlinear Analyses, *Computational Mechanics,* 51, 2013, pp. 843–864. doi: 10.1007/s00466-012-0762-2.
11. Yang, Y., Tang, X.H., and Hong, Z., A Three-node Triangular Element with Continuous Nodal Stress, *Computers and Structures,* 141, 2014, pp. 46-58. doi: 10.1016/j.compstruc.2014.05.001.
12. Yang, Y., Xu, D., and Zheng, H., Application of the Three-node Triangular Element with Continuous Nodal Stress for Free Vibration Analysis, *Computers and Structures,* 169, 2016, pp. 69-80. doi: 10.1016/j.compstruc.2016.03.008.
13. Yang, Y. and Zheng, H., A Three-node Triangular Element Fitted to Numerical Manifold Method with Continuous Nodal Stress for Crack Analysis, *Engineering Fracture Mechanics,* 162, 2016, pp. 51–75. doi: 10.1016/j.engfracmech.2016.05.007.
14. Sun, G., Yang, Y., and Hong, Z., A Three-Node Triangular Element with Continuous Nodal Stress (Trig3-CNS) for Geometry Nonlinear Solid Mechanics Problems, *International Journal of Computational Methods,* 15(1), 2018, pp. 1850022 (1-21). doi: 10.1142/s0219876218500226.
15. Wong, F.T., Soetanto, R., and Budiman, J., On the Accuracy and Convergence of the Hybrid FE-meshfree Q4-CNS Element in Surface Fitting Problems, *MATEC Web* Conferences, 147, 2018, pp. 1-7. doi: 10.1051/matecconf/201814701002.
16. Wong, F.T. and Kanok-Nukulchai, W., Kriging-based Finite Element Method: Element-by-element Kriging Interpolation, *Civil Engineering Dimension,* 11(1), 2009, pp. 15–22.
17. Zheng, C., Tang, X.H., Zhang, J.H., and Wu, S.C., A Novel Mesh-free Poly-cell Galerkin Method, *Acta Mechanica Sinica,* 25, 2009, pp. 517–527. doi: 10.1007/s10409-009-0239-5.
18. Wong, F.T. and Kanok-Nukulchai, W., On the Convergence of the Kriging-based Finite Element Method, *International Journal of Computational Methods,* 06(01), 2009, pp. 93-118. doi: 10.1142/s0219876209001784.
19. Bathe, K.J., *Finite Element Procedures*, Prentice Hall, Pearson Education, Inc., 1996.

20. Zienkiewicz, O.C. and Taylor, R.L., *The Finite Element Method, Volume 1: The Basis*, Fifth Edition, Barcelona, Spain: The International Centre for Numerical Methods in Engineering, 2000.